Edelweiss Applied Science and Technology
ISSN: 2576-8484
Vol. 8, No. 6, 8126-8149
2024
Publisher: Learning Gate
DOI: 10.55214/25768484.v8i6.3757

Thermal-Fluid study of curved tubes in cross-flow

Kunal[1], Sushil Kumar Dhiman[2*]
[1,2]Department of Mechanical Engineering, Birla Institute of Technology, Mesra, Ranchi (India); kunalkumar71@yahoo.in (K.) skdhiman@bitmesra.ac.in (S.K.D.)

Abstract: Three-dimensional simulations have been performed to investigate thermal performance by the external surface of curved circular tubes provided with concave and convex curvatures. The simulations were performed in Ansys-fluent software and results has been validated against the available results. The tubes were placed in a uni-directional free stream of air at a Reynolds number of 35000 which is within subcritical range for circular tube. The heat transfer capabilities of curved tubes have been compared with that of a straight tube of same diameter and height. A constant-heat-flux condition over the external surface has been used. The curved tubes have been designed such that it has vertical extensions at the end and curvatures at the middle section with curvature ratios of 0.075, 0.15, 0.225 and 0.3. Plots of coefficients of pressure, drag and lift, Nusselt number, heat transfer ratio and contours of pathlines were utilized to investigate the thermal behaviour around the tube surface. Results show the highest augmenting thermal performance exhibited by convex curved tube with curvature ratio 0.15 followed by curvature ratio of 0.225. Other reasonably better augmented heat transfer exhibited by concave curved tube with curvature ratio of 0.3. The present study also identifies augmenting, mitigating and insignificant zones around the tubes based on heat transfer rates. The results show an improvement in heat transfer when curved tube is used instead of straight tube which can be utilised in waste heat recovery recuperators.

Keywords: *Augmenting, mitigating and insignificant zones, Curvature ratios, Heat transfer capabilities, Straight and curved tubes, Surface fraction, Zones of influence..*

1. Introduction

Heat transfer capabilities from the outer surface of tubes using air as energy carrier have been the topic of research since many decades. Researchers have been involved in observing possibilities to extract unutilized heat in industrial applications, for instance the heat recovery using recuperators [1]. Augmentation or optimum utilization of heat transfer is usually the prime concern as far as the economic operation and environment protection is taken care off. Hence, many trials had been conducted to investigate enhanced capabilities from external surface of tube based on the shape and structure of a straight tube [2-7], and also for the oscillations of straight tube as well as heat carrier fluid type [8-10]. However, fluid dynamics of oil risers in marine application [11] motivates the investigation of passive heat transfer capabilities from curved tubes. In recent days from various trials of recuperators by the manufacturing industries, the use of curved tubes has pulled attentions to explore the heat transfer capabilities for waste heat recovery applications. Unfortunately, there is gap of findings in this research field. It is a well-known fact that the wake region of the tubes has significance as it leads to release of vortices that has shedding tendency and generates sweeping action over the tube surface that attends the wake. Chiatto et al. [12] have studied the properties of wake flow behind curved tubes. Effect of Reynolds number, aspect ratio and angle of curvatsure were discussed. For low aspect ratio, single oblique shedding was seen and for higher aspect ratio both normal and oblique shedding regime was present. Increase in curvature resulted in flow-transition taking place at higher Reynolds number. Jiang et al. [13] have investigated the wake of quarter ring concave type curved cylinder and found that vertical and horizontal extensions have significant effect on flow. Investigation of Gallardo et al. [14] on a quarter ring shaped circular tube kept in convex manner in the flow shows a contrast shedding of vortices from upper and

* Correspondence: skdhiman@bitmesra.ac.in

lower segment of the tube. The vortices in the upper portion of the tube were more coherent and that in lower portion was supressed and lacked coherence. Miliou et al. [15] computationally studied the fluctuating forces and vortex core in wake region. Effect of length of horizontal extension was studied and found that an extension of ten times of diameter resulted in less vigorous shedding. Isolated tube and bounded tube behave differently and its impact in heat transfer is different. Further, Miliou [16] found a dominant shedding from the top of convex type curved cylinder but in concave type curved cylinder no shedding to mild shedding was found. Total drag was reduced in case of concave cylinder as a result of this reduction in shedding. A wind tunnel test was performed by Yemenici and Umur [17] for convex and curved surfaces under three distinct flows viz. laminar, transition and turbulent, where concave surface showed heat transfer augmentation while convex surface showed a mitigation. Can et al. [18] investigated the heat transfer in curved tubes with varying curvatures in terms of curvature ratios for a range of Reynolds number between $4x10^4$ and $40x10^4$. Both concave and convex curvatures showed higher heat transport for high Re's. A rise in Nu with increasing curvature in convex cases is due to accelerating flow from front stagnation point and for concave cases due to boundary layer thinning effected by enforced curvature and vortex generation. A 3-D computational work of Gao et al. [19] for a flow over two circular cylinders provided with convex curvature and placed side-by-side was reported for investigation of effect of varying spacing ratios and low Re. The investigation identified four distinct flow patterns and five distinct flow regimes. Aasland et al. [20] have investigated the transport of heat from two circular cylinders placed in tandem and provided curvature of convex based on flow direction. Many regimes in flow were identified when spacing ratio between them was varied. Negligible drag was reported for downstream cylinder which was attributed due to a significant suction pressure within the gap between them. Also reported a low lift on cylinder at upstream because for formation of quasi stationary vortices. A concave and convex plane surface were studied by Mayle et al [21] to investigate turbulent boundary layer heat transfer and reported a maximum heat transfer in concave surface over convex surface.

Difficulties in the fabrication of precise complex geometry of the body kept in the flow orients the research to the computational studies. Dhiman et al.[22] has reported in the review that the suitable numerical schemes and turbulence model are dependent on the order of accuracy of derivatives and gradients along with the mesh management. Heat transfer capabilities of wall function in turbulence models is low while Wolfstein's near wall treatment has good capabilities. k-ε is favourable for characteristics estimation of flow dynamics while SST k-ω is very close predictions of thermo-fluid characteristics. Paul et al. [23] compared four different turbulence model in tube bundles and found that k- based equation model predicted Reynolds normal stress better than the ε-based second closure while ω-based models precisely predict mean velocity compared to other models. Numerous benchmark heat transfer based experimental and numerical investigations, such as Tsutsui and Igarashi [24], Nakamura and Igarashi [25], Dhiman et al. [26, 27], Igarashi [28], Sanitjai and Goldstein [10], was conducted on external cross-flow over the tubes or cylinders. Over a wide subcritical range of Re these reports show various empirical relations and flow regimes from where estimations and augmentation of heat transfer can be identified. In addition, various inverse heat conduction numerical approaches have been reported in Roy and Dhiman [29], Dhiman and Prasad [30] for the heat transfer analysis from external flow from straight tube.

Looking forward to embrace enhanced surface area by providing curvatures on circular tube along the length. It influences the flow structures around its surface which has encouraged to conduct a literature survey. From the entire review of literatures, including state of the art, it has been observed that the heat transfer capabilities from the curved tubes subjected to uni-directional free stream of air as heat carrier fluid had not been investigated. A few literatures were observed which shows studies on fluid dynamics for partial curvature to the tube such as elbow type or raiser, etc, it however, does not contain heat transfer study. In the present study, a smooth symmetrical curvature has been provided on the circular tube with different curvature ratios. Depending upon the flow direction of fluid, the tube's leading generator may receive fluid in a concave or convex manner. The objective was to investigate the thermal performance of the curved tubes and to compare it with straight tube. Also, the influence of various curvature ratios provided to the tube on flow and heat transfer characteristics was aimed to investigate. The study was conducted computationally using three-dimensional modelling with proper validation of numerical scheme. The transition in boundary layer phenomenon in the numerical scheme has been utilized which is also the novel work that make use of three-equation turbulence model *k-kl-ω* because the Re=35000 lies in subcritical range of tube.

1.1. Numerical Scheme, Computational Model and Validations:

The present computations follow analysis of unsteady characteristics in an incompressible flow air past curved and straight circular tubes. Tube surface is given a constant-heat-flux condition and the uni-directional free stream velocity at the inlet is so given that the Reynolds number based on diameter approached 35000. Because Reynolds number lies in the subcritical range of tubes, a transition sensitive eddy-viscosity type three equation *k-kl-ω* model Walters and Cokljat [31] has been utilized. The model predicts a precise flow and heat transfer characteristics at the wall interacting with fluid, however, shows few limitations such as fine and structured mesh, laminar kinetic energy growth in the far-field, and at some occasions the flow reversals which may be resolved by the relaxation parameters. The equations that govern the present flow problem have been summarised as follows:

1.1.1. Continuity Equation:

$$\frac{\partial \rho}{\partial \tau} + \nabla\left(\rho \bar{V}\right) = 0$$

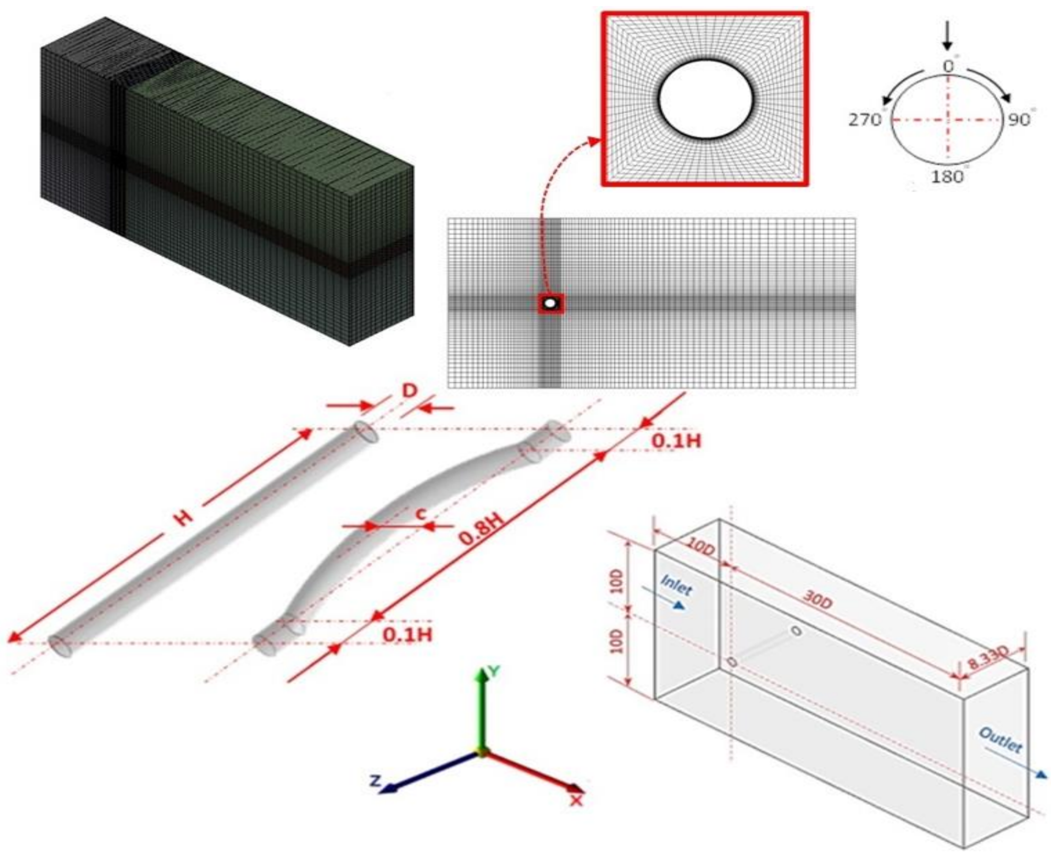

Figure 1.
Schematic of computational domain with boundary conditions and grid resolution.

1.1.2. N-S equation

$$\frac{D\overline{V}}{D\tau} = \frac{-1}{\rho}\nabla p + \nu\nabla^2\overline{V}$$

The NS equation is further modified as

$$\frac{D\overline{V}}{D\tau} = \frac{-1}{\rho}\nabla p + \nabla\left[\overline{V}\left(\nabla\overline{V} - \overline{u_m u_n}\right)\right]$$

where $-\overline{u_m u_n}$ is the turbulent stress term represented by Boussinesq equation. For instance for the x-momentum equation turbulent stress terms is represented as $-\overline{u_i u_j} = \nu_{tot}\left(\frac{\partial V_i}{\partial y} + \frac{\partial V_j}{\partial x}\right) - \frac{2}{3}k_{tot}\delta_{i,j}$, where v_{tot} is total kinematic eddy viscosity and k_{tot} is the total turbulent kinetic energy. Note that the k_{tot} considers laminar energies and large scale as well as small scale turbulent energies.

In the equation, m or n represents i or j or k based on matched or unmatched derivative terms with the direction of equation, however, for the matched derivative terms with the direction of equation $m=n$ for which $-\overline{u_m u_n} = 0$

1.1.3. Energy equation

$$\frac{De}{D\tau} = \alpha\, c_p\nabla^2 T \quad ,where \quad e = \overline{V}\ \nabla\left(c_p T\right)c$$

The governing equations considers the energy balance under constant fluid property and negligible volumetric heating as well as viscous energy dissipation in an incompressible flow.

The energy equation in terms of T may be modified as:

$$\frac{DT}{D\tau} = \nabla\left(\alpha\ \nabla T - \overline{u_m\zeta}\right)$$

where $-\overline{u_m\zeta}$ is the Fourier's relation, for instance for $m = i$, $-\overline{u_m\zeta} = \alpha_{\zeta,tot}(\partial T/\partial x_i)$ and $-\overline{u_m\zeta} = 0$ for the y and z derivatives. The equations consider ζ_{tot} represents temperature fluctuations and $\alpha_{\zeta,tot}$ total thermal diffusivity

Boundary conditions: Tube surface has been provided with no-slip ($u=v=w=0$) and constant-heat-flux (q_w=constant) conditions. Uni-directional velocity $\overline{V} = u$ has been provided at the inlet section of the flow domain along x-direction with thermo-physical properties of air at 300K. At the outlet an outflow condition has been provided with first order accuracy.

The various dimensionless parameters which are the coefficients of drag (C_D), lift (C_L) and pressure (C_p) were monitored for a stable solution and the residuals were monitored for accuracy of less than 10^{-3} ensuring convergence. The flow time has been represented by ξ. A high frequency vortex shedding was analysed using power spectral density whose Fast Fourier Transformation provided the Strouhal number (St). Following are formulation of dimensionless parameters used for the analysis in the present paper.

$$C_D = \frac{2F_x}{\rho\overline{\overline{V}}^2 A} = -\frac{1}{2}\int_0^{2\pi} C_p\cos\theta\, d\theta$$

$$C_L = \frac{2F_y}{\rho\overline{\overline{V}}^2 A}$$

$$C_p = \frac{p - p_\infty}{\frac{1}{2}\rho \overline{V}^2}$$

$$\xi = \frac{t\overline{V}}{D}$$ *, where t is computational time*

$$St = \frac{fD}{\overline{V}}$$

$$Nu_\theta = \frac{1}{\xi}\int Nu'_\theta(\xi)d\xi$$ *, time averaged local Nusselt number*

Table 1.
Various grid sizes and time steps for grid independence test.

Case no.	Times steps	Minimum cell distance	Cell counts	C_L	C_D	Nu_m
1	10^{-4}	$1.3x10^{-5}$	322290	± 1.19	1.16	140.0
2	10^{-4}	$1.3x10^{-5}$	403648	± 1.40	1.35	162.77
3	10^{-4}	$1.3x10^{-5}$	504840	± 1.48	1.39	162.50
4	10^{-4}	$1.3x10^{-5}$	631040	± 1.48	1.39	162.10
5	$5x10^{-4}$	$1.3x10^{-5}$	631040	±1.18	1.48	142.21
6	$5x10^{-4}$	$6.5x10^{-5}$	794848	± 1.6	1.45	139.43
7	10^{-3}	$1.3x10^{-5}$	403648	± 1.52	1.75	170.56
8	10^{-3}	$1.3x10^{-5}$	503678	± 1.75	1.75	154.32
9	10^{-3}	$6.5x10^{-5}$	503678	± 1.75	1.45	178.12

Table 2.
Various grid sizes and time steps for grid independence test.

Authors	C_L	C_D	Nu_m
Present study	1.39	± 1.48	162.5
Perkins and Leppert (1964)[32]	--	--	156
Hishikar et al. (2023)[1]	1.38	± 1.46	156.10
Sanitjai and Goldstein (2004)[10]	--	--	136

Edelweiss Applied Science and Technology
ISSN: 2576-8484
Vol. 8, No. 6: 8126-8149, 2024
DOI: 10.55214/25768484.v8i6.3757

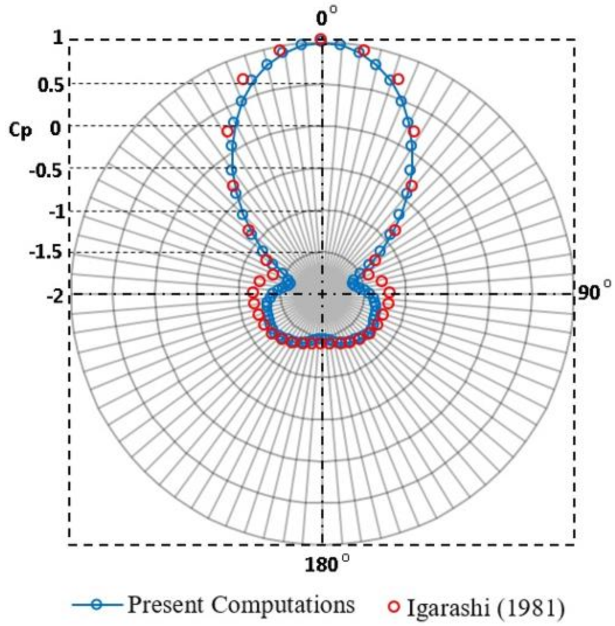

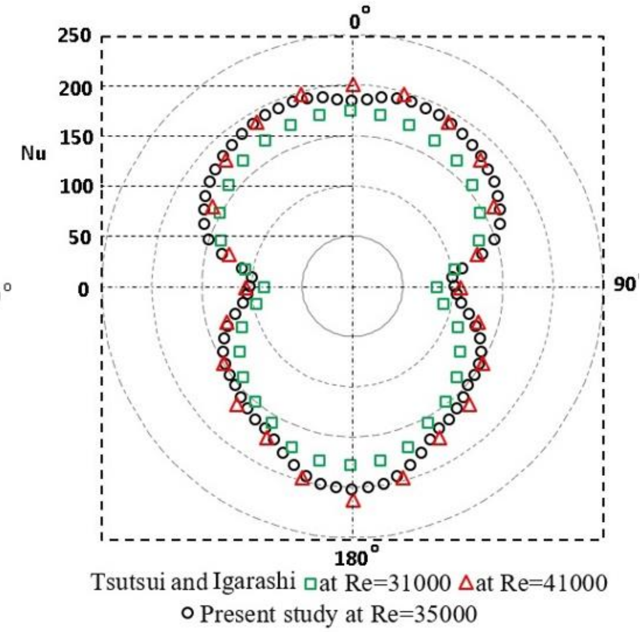

Figure 2.

Comparison of time-averaged Cp distribution around tube at the central plane at Re=35000 with Igarashi [33] and comparison of time averaged Nu distribution around tube at the central plane at Re=35000 from present computations, at Re = 31000 and Re = 41000 from Tsutsui and Igarashi [24].

Computational model: A rectangular cuboidal form of fluid domain of size 40Dx20Dx8.33D was created as shown in Fig.1 whose length was taken along *x*-direction with broader rectangular surfaces parallel to *x,y*-plane while thickness was taken along z-direction. A tube of 30mm diameter (D) was placed perpendicular to *x,y*-plane which was located 10D from inlet, top and bottom side surfaces and 30D from outlet. Tube height was 8.33D and its ends touch the wall of symmetry. Structured grid with hexahedral cells was created in the fluid domain. A high-resolution fine mesh was created close to the tube surface with minimum cell size of 0.00043D that grows smoothly and uniformly to all extents of fluid domain. The inlet surface was given a uni-directional velocity, all side-surfaces were given symmetric boundary condition, outlet surface was given outflow condition, and tube surfaces was given a wall boundary condition with no slip. A parabolic criterion of solving algebraic equations was followed at all nodes for the estimation of pressure and velocity. Pressure-based transient time marching solver was implemented with time steps of 10^{-4} using time stepping by implicit criteria based on backward Euler method. Derivatives and gradients were estimated by least square cell-based theorem that increases the accuracy of the estimates. Discretization of pressure was done by Standard method while coupling of pressure-velocity by SIMPLEC algorithm was followed. Entire momentum equations were solved by second order accuracy while the laminar as well as large and small scale turbulent energy equations were solved by second order accuracy with upwinding scheme.

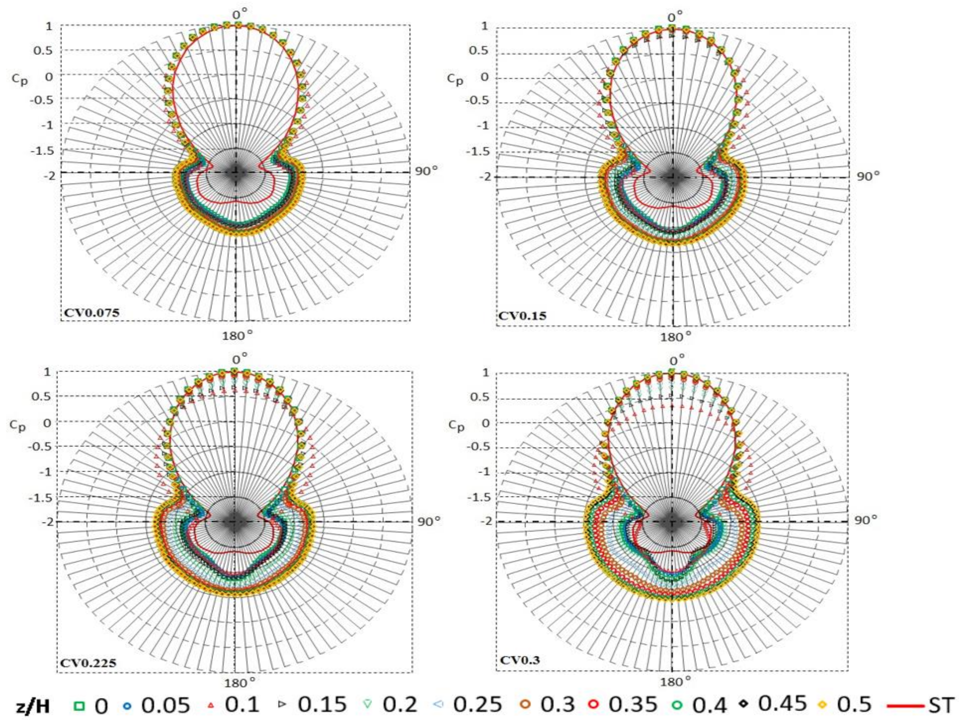

Figure 3.

(a) Comparison of Cp distribution of CV 0.075 to CV 0.3 at 0⩽z/H⩽ 0.5.

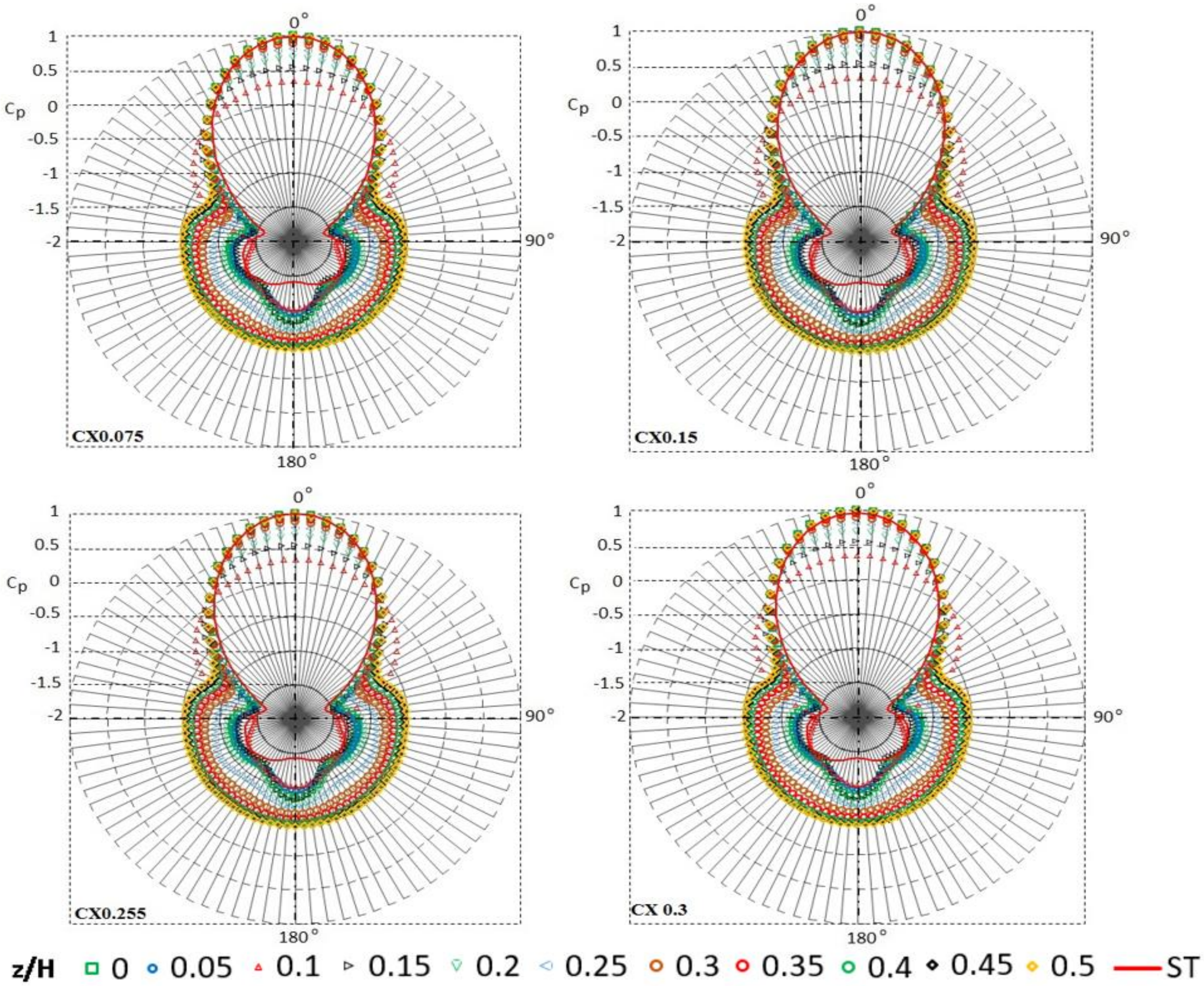

Figure 3.

(b) Comparison of Cp distribution of CX 0.075 to CX 0.3 at 0⩽z/H⩽ 0.5.

Grid independence test and validation: A grid independence test was performed on straight tube prior to finalize the entire computational scheme for which benchmark literature's data has been utilized for the validation study of the present work. Table 1 depicts times steps, minimum cell size and cell counts along with C_D C_L, Nu_m (time averaged mean Nusselt number). Table 2 depicts a comparison of C_D, C_L, Nu_m of the present computations with the benchmark literature. Out of many more trials a few data that shows close outcome have been shown in Table 1 where case no. 3 has been observed as a best fit.

The present computation's outcome was found in close agreement with the reported data from the literatures as shown in Table 2. Fig 2 shows the comparisons of time averaged pressure distribution as well as Nusselt number distribution at the central plane of the straight tube. The comparisons were done with various benchmark data literatures. A reasonably good validation was observed with percentage

ISSN: 2576-8484
Vol. 8, No. 6: 8126-8149, 2024
DOI: 10.55214/25768484.v8i6.3757

deviations of less than 0.7% over the entire Cp distribution, while for Nu the present computation lies in good proximity within the distribution at Re of 31000 and 41000. Evidently Tables 1 and 2 and Figures 2 (a) and (b) sufficiently proves the validity of the present computations, hence the entire three-dimensional modelling and computations were conducted with the present scheme whose results and discussion have been presented in the subsequent section.

2. Results and Discussion

The time averaged pressure distribution in terms of pressure coefficient (Cp) has been represented in the Figs 3(a) and 3(b) for curved tube with concave curvature (CV) and that with convex curvature (CX) respectively for various heights (z/H) from lower end at various curvature ratios CR = c/L. Different CR used for both CV and CX are 0.075, 0.15, 0.225, and 0.3. Each figure can be identified by the name CV or CX followed by a curvature ratio, for example curved tube with concave curvature (CV) and curvature ratio CR=0.075 is represented as CV0.075. The pattern of Cp-distribution on curved tube for each CR and z/H is similar to that of straight tube (ST), however the flow separation points vary for each of the cases showing early separations in curved tube compared to that of straight tube. This causes relatively enlarged vortex flow zones on their downstream portions of the curved tubes. Enlarged vortex flow zones resulted in reduced suction pressure distributions in the separated zone compared to that of ST. This also causes a reduction in the overall drag on curved tubes and reduces the transverse movements of vortex shedding, which appears as low lift coefficients (C_L). Consequently, the overall phenomenon enhances the possibilities for augmentation in heat transfer compared to straight tube.

Nu-distribution around the CV and CX tubes for various dimensionless heights (z/H) from one end at various curvature ratios CR have been shown in Fig 4(a) and 4(b) respectively. The distributions are axisymmetric and all the Nu-distribution plots also contain distribution of ST so that a comparison of heat transfer rate can be made. All the figures illustrate that providing curves in tube alters heat transfer, nevertheless, the change in CR ratio has major effect on heat transfer on the separated portion of tube. It can broadly be seen by focusing the separated zone that the CR for CX tube establishes a constraint upto CR=0.225 beyond which the heat transfer reduces below that of the ST tube. In case of CV tube, no such constraint has been observed for CR till 0.3 as for almost all z/H the heat transfer is higher than that of the ST. Additionally, it shows a regular improvement in heat transfer with increase in CR. It can also be clearly observed that the zone of influence (ZI) for heat transfer is different at different z/H of different CRs and it is curvature dependant i.e. CV or CX. The ZI is called to be zone of augmenting influence (ZAI) when there is an improvement in heat transfer over that of the ST whereas the ZI is called as zone of mitigating influence (ZMI) when there is deterioration in heat transfer relative to the ST. Also, the zone for which no influence is seen compared to ST has been referred as zone of insignificant influence (ZII). For instance, in case of standalone ST the ZAI is for the range 87°-274° over the separated flow regime because the heat transfer starts to increase after achieving the minimum value while ZMI is for the range 274°-87° over the attached flow regime. For CX with CR=0.075 (CX 0.075) at z/H =0.5 there are four ZAIs on the separated portion i.e. 86°-118°, 140°-160°, 200°-220°, and 242°-274°, it has two ZIIs 118°-140° and 220°-242°, while over the attached flow regime it has one ZAI for the range 290°-70° (i.e. between ±70°) and two ZMIs for the ranges 70°-87° and 273°-290°. Consequently, CX 0.075 at z/H =0.5 shows overall aggravating influence.

The separated regime of the case of CX 0.075 shows that the heat transfer rate is least augmented at the middle plane where z/H=0.5 and successively improving augmented with change of z/H toward the tube ends. However, the separated regime of the cases CX0.15 and CX0.225CX shows a reverse tendency of heat transfer rate, where it is most augmented at the middle plane i.e. at z/H=0.5 and successively deteriorates in augmentation of heat transfer with change in z/H toward the tube ends. Nevertheless, the separated regime of the case CX0.3 shows the mitigating tendency of heat transfer rate compared to that of ST. The separated regimes of cases CV0.075 and CV0.15 does not show a substantial augmentation in heat transfer and so the entire range of z/H for both cases can be kept under classification of ZII. The separated regime of case CV0.225 shows mitigating tendency in the central zone for about 50% of the entire height of curved tube with least heat transfer in the central plane and minor improvements away from the central plane, followed by an FII zone around z/H=0.3 and thereby augmentation in heat transfer commences which goes on improving till the tube ends at z/H=0.1 and 0.9. The separated regimes of case CV0.3 shows a further improvement compared to CV0.225 with mitigating tendency of heat transfer reduced to about 25% of the entire height of curved tube with least heat transfer in the central plane and getting improvised away from the central plane showing ZII at about z/H = 0.35 followed by major augmentation in heat transfer towards the tube ends.

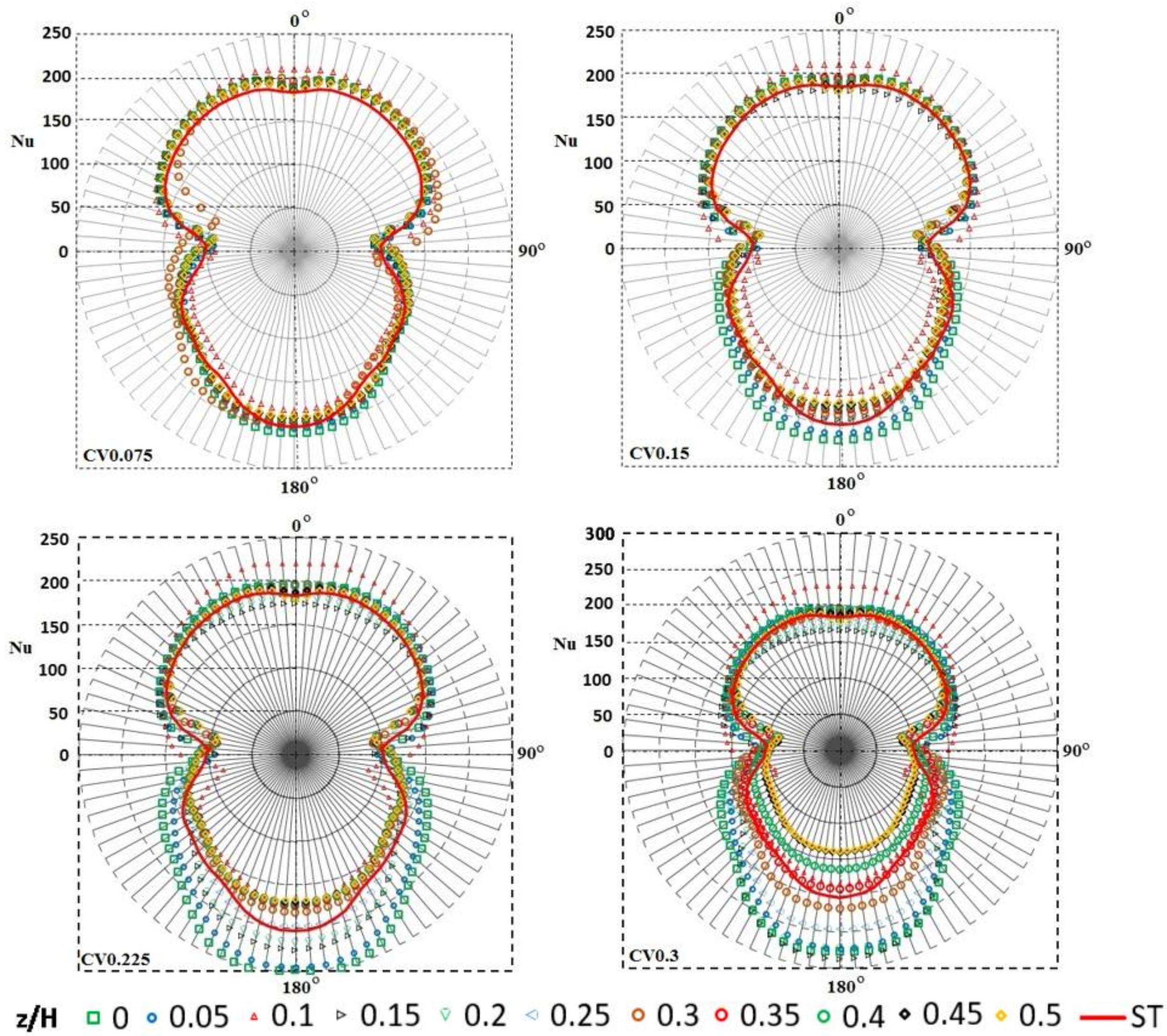

Figure 4.
(a) Comparison of Nu distribution of CV 0.075 to CV 0.3 at 0⩽z/H⩽ 0.5.

Edelweiss Applied Science and Technology
ISSN: 2576-8484
Vol. 8, No. 6: 8126-8149, 2024
DOI: 10.55214/25768484.v8i6.3757

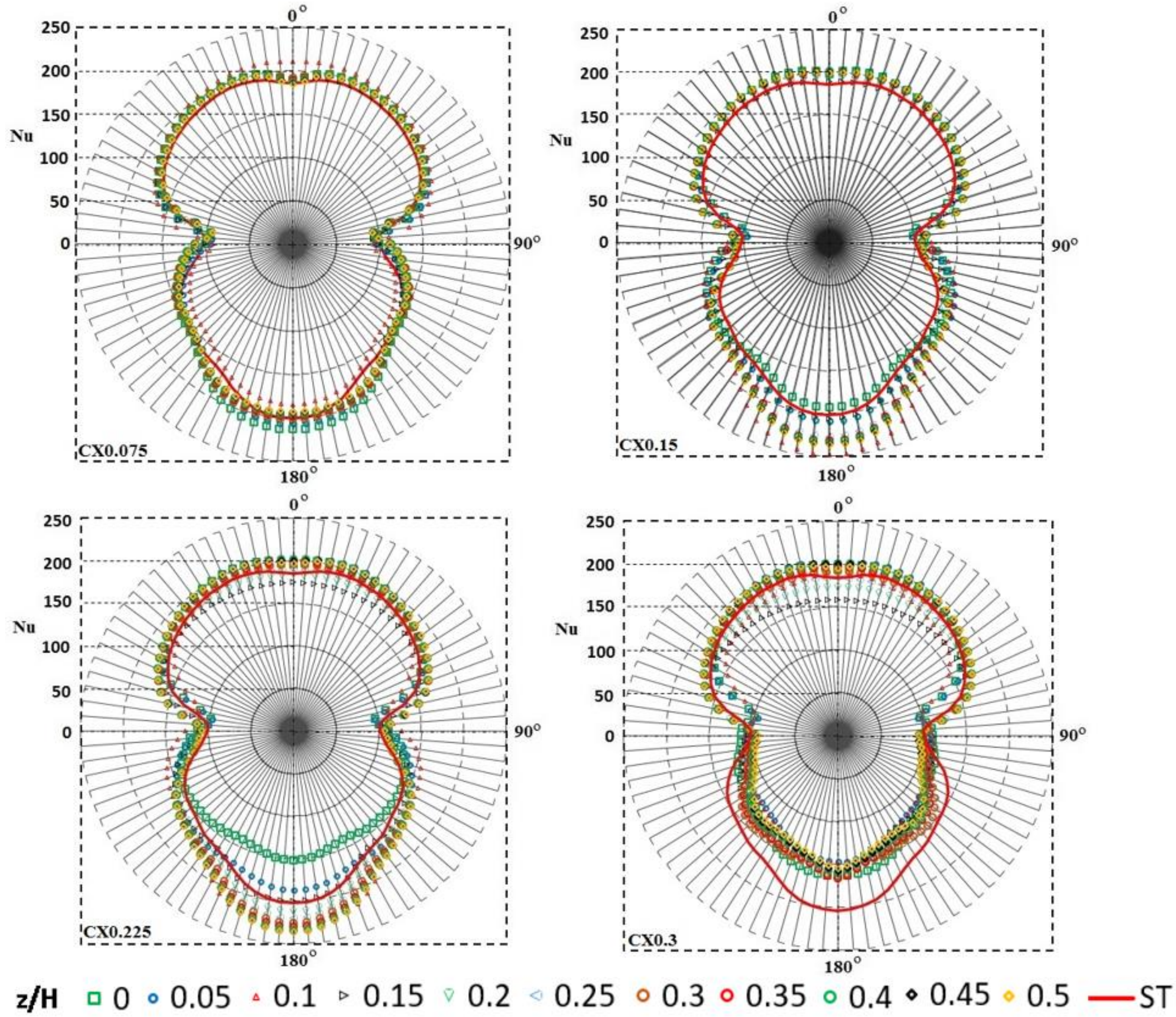

Figure 4.
(b) Comparison of Nu distribution of CX 0.075 to CX 0.3 at 0⩽z/H⩽ 0.5.

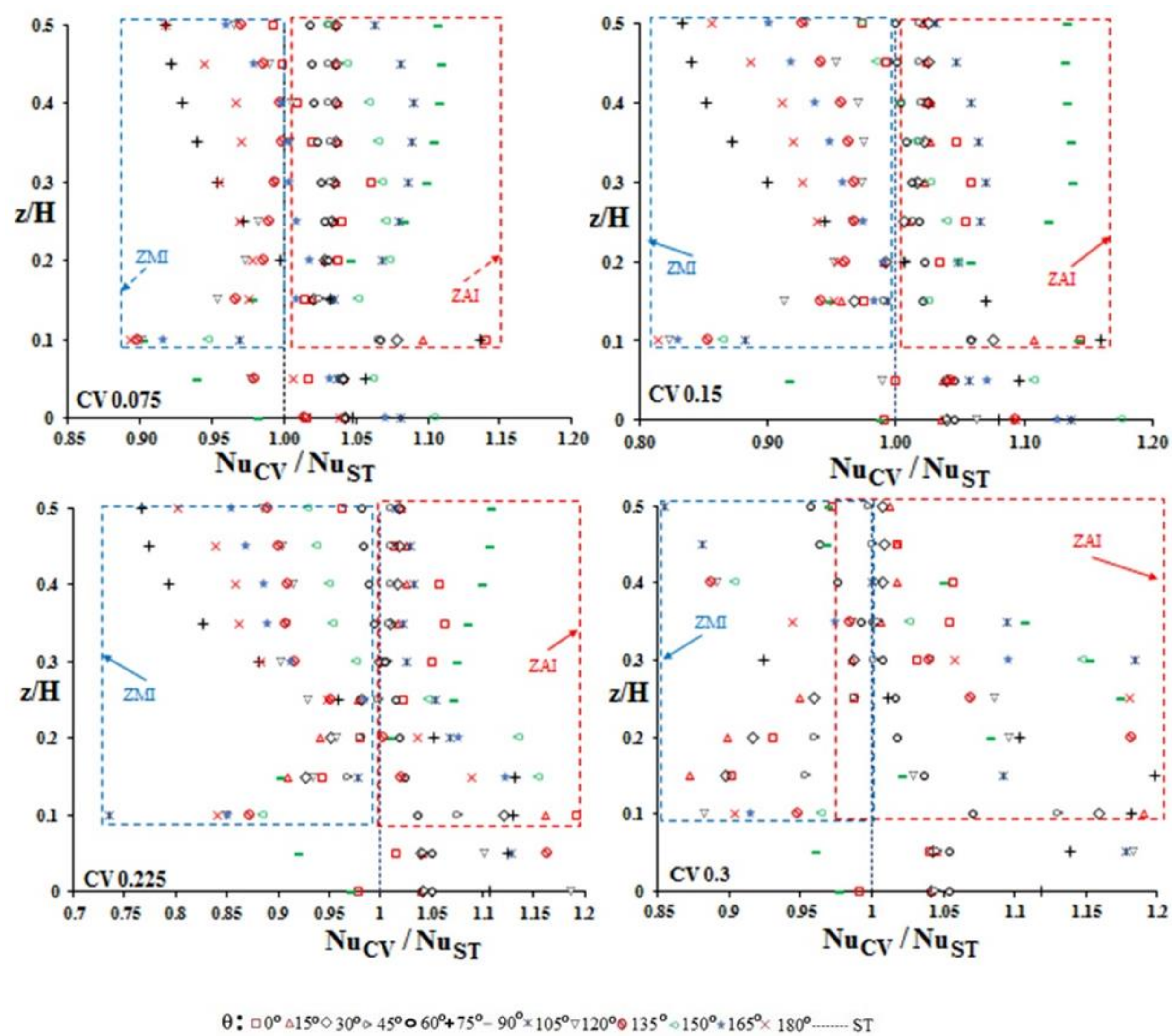

Figure 5.
(a) Comparison of Nu_{CV}/Nu_{ST} of CV 0.075 to CV 0.3 at $0 \leqslant z/H \leqslant 0.5$ on zone basis.

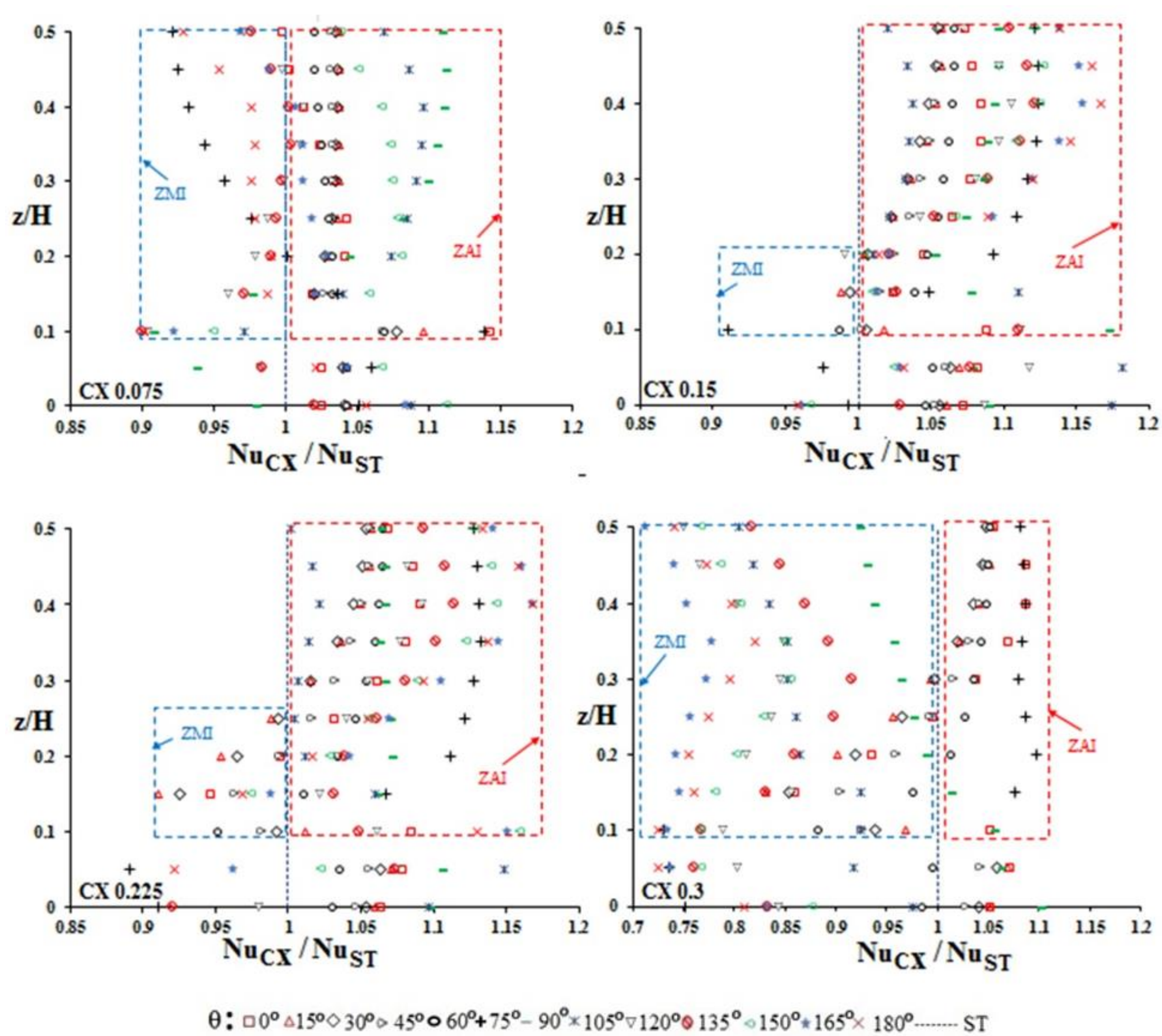

Figure 5.
(b) Comparison of Nu_{CX}/Nu_{ST} of CX 0.075 to CX 0.3 at $0 \leqslant z/H \leqslant 0.5$ on zone basis.

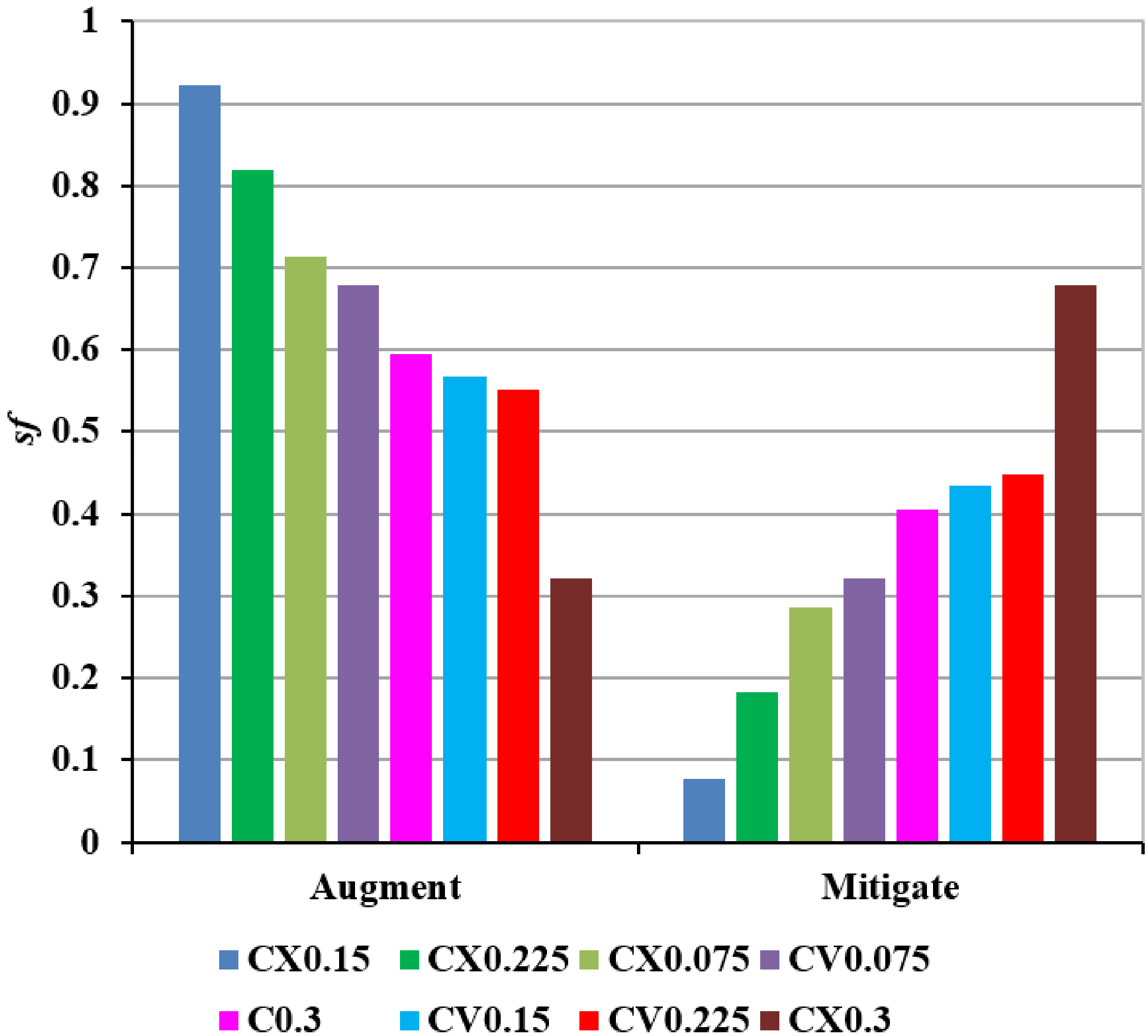

Figure 6.
Fraction of tube surface representing the Augmenting and Mitigating zones over the entire surface of curved tubes of Nu_{CX}/Nu_{ST} of CX 0.075 to CX 0.3 at $0 \leqslant z/H \leqslant 0.5$ on zone basis.

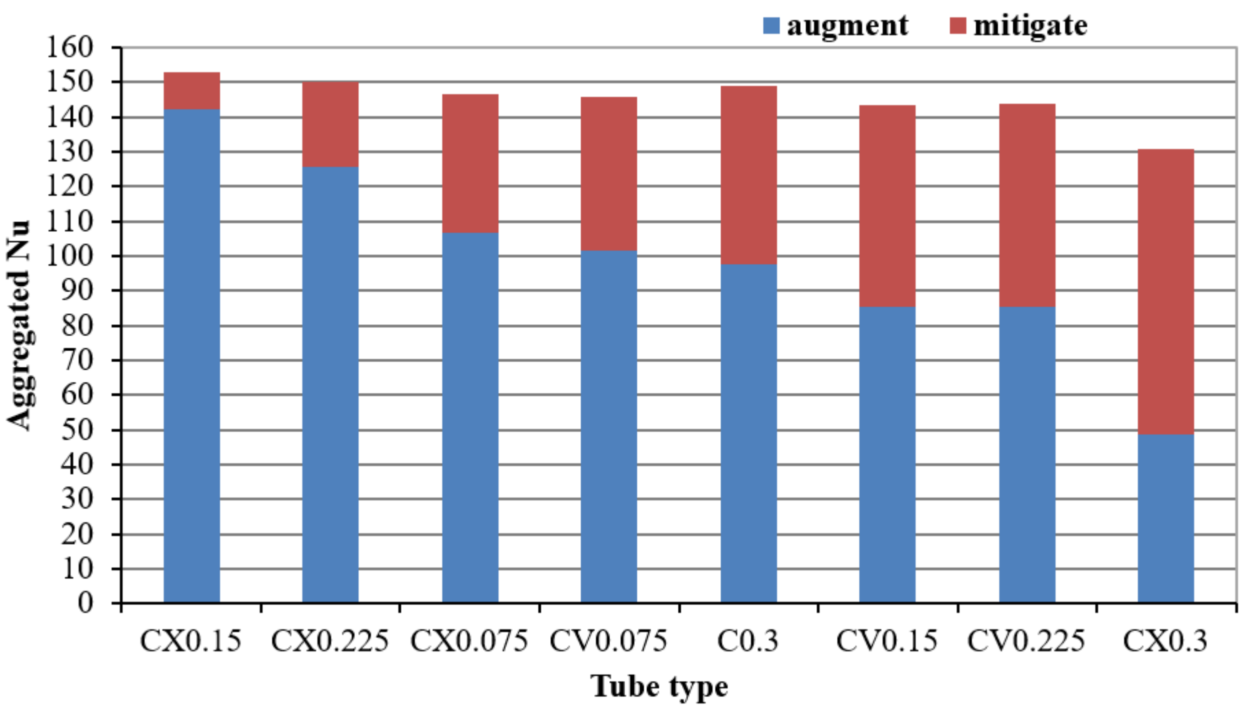

Figure 7.
Aggregates of heat transfer ratio in Augmented vs Mitigated zones for curved tubes.

The overall observation on CR and z/H also shows that the heat transfer is improved a little in CV cases and improved considerably in CX cases of curved tube compared to that of ST over the attached flow regimes of the tubes.

A further study of thermal performance based on a systematically organised numerous nodes over the surface of each curved tube has been presented. The Fig 5(a) and 5(b) can be referred for the zonal study over the entire surface of each curved tube. The figures illustrate the fractional values of heat transfer, called as HTR, the Heat Transfer Ratio, based on heat transfer data of ST on the respective zones which is represented on abscissa and have been compared against z/H for various angular location with respect to front stagnation point. Figure shows a vertical line at $Nu_{CX}/Nu_{ST} = 1$ or $Nu_{CV}/Nu_{ST} = 1$ that represents the line of comparison of the thermal performance of various node locations on the surface of curved tube. The figures also show demarcated ZAI and ZMI zones that illustrates number of nodes lying in demarcated portions which helped to analyse the area weighted surface fraction (*sf*) of tube based on heat transfer, as shown in Fig. 6, that represents the augmenting and mitigating zones over the entire surface. The *sf* >0.5 for augmented zone is an indicative of augmented thermal performance. Consequently, CX0.15 with *sf* >0.9 for augmented zone was expected to give highest thermal performance while CX0.3 with *sf <0.35* for augmented zone was expected to give least thermal performance. The number of nodes lying into the demarcated portions also helped to evaluate aggregate HTR for various cases of curved tube. It is observed that CX has majority of nodes lying ZAI which is highest in CX0.15 followed by CX0.225 and CX0.075 but the CX0.3 shows a contrary behaviour with majority of the nodes lying in the ZMI. Also, all the cases of CV show majority of the nodes lying in the ZAI however the difference in their counts between ZAI and ZMI is low. Nevertheless, the node in the ZAI should also exhibit significant transfer ratio then only a considerable aggregate of HTR can be achieved. Hence, the aggregate HTR for augmented and mitigated zones have been analysed and has been represented in the Fig 7. The aggregate HTR in augmented and mitigated zones clearly indicates that CX0.15 exhibit highest augmented zones with gradually subsiding augmented zones in sequence as observation also holds for rising trends of mitigated zones. It shows that there is no fixed trend of CR, however, CX with CR<0.3 is favourable for reasonably good augmentation in heat transfer as a stand-alone tube. A comparison of aggregate HTR for tube with curvatures with that of ST integrating both augmented and mitigated zones has been illustrated in Fig. 8. The figure shows an interesting observation that although the CX0.075 and CV0.075 exhibits a relatively higher nodes in ZAI compared to that of CV0.3, the aggregates obtained on integrating both augmented and mitigated zones shows higher HTR for CV0.3 compared to that of CX0.075 and CV0.075. This is due to the fact of attaining relatively higher HTR at individual nodes makes the better effectiveness of overall thermal performance. The figure also illustrates that the highest thermal performance exhibited by CX0.15 followed by yet another good thermal performance by CX0.225 and CV0.3. The cases of CX0.075 and CV0.075 also show a better HTR compared to that of ST. The cases of CV0.15 and CV0.225 show insignificant thermal performance, while the case of CX0.3 does not show augmentation in thermal performance rather it shows mitigation.

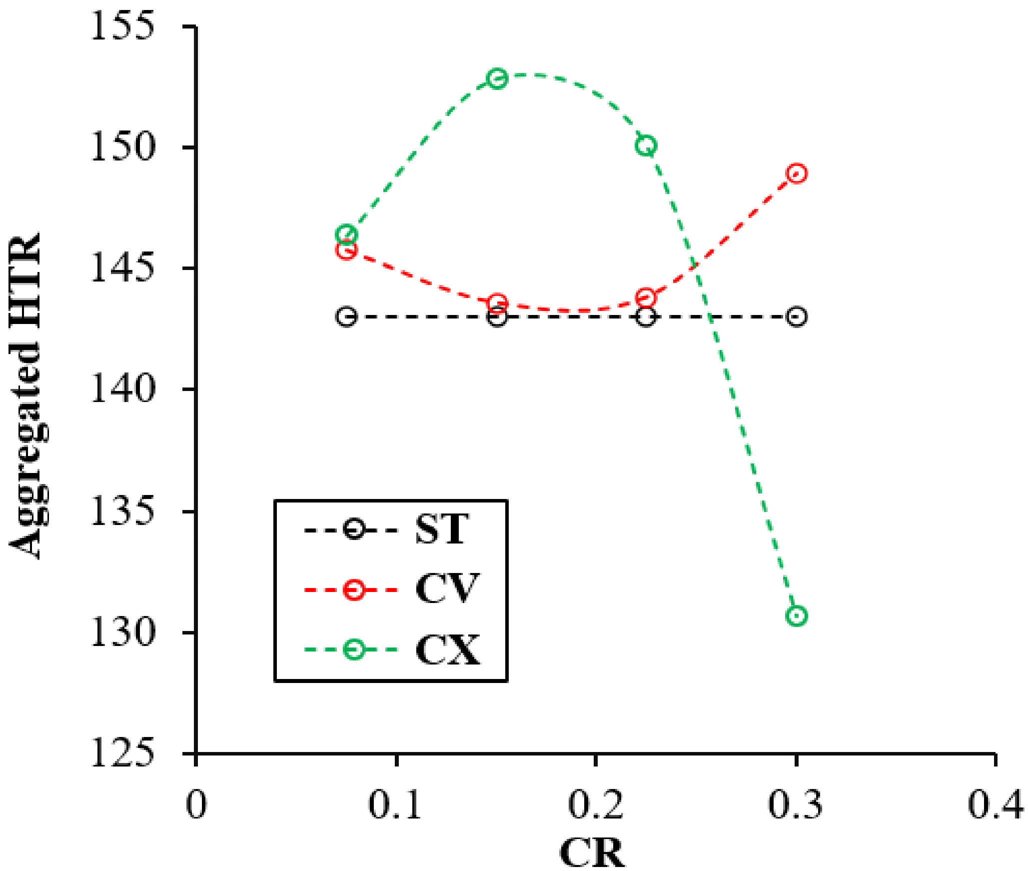

Figure 8.
Comparison of aggregates of HTR for curved tubes with that of ST integrating augmented and mitigated zones.

Drag (C_D) and lift (C_L) coefficients were monitored over the non-dimensional computational time (ξ) that has been represented in Fig 9. Contours of pathlines for ST and all CVs and CXs have been shown in Fig 10. Contours of pathlines shows that in case of ST the fluid structures spread uniformly over the entire span of tube but a little inward curvature as given in CV0.075 produces slight suction heading to the central plane. Hence, the fluid structures tend to shift a little towards central plane resulting in drag reduction by about 30% and that greatly reduce the strength of vortex shedding with unchanged shedding frequency. With further increase of curvature to CV0.15, CV0.225 and CV0.3, a successively more agglomerating shift of vortex structures heading to central plane exhibits an additional drag reduction with unchanged low strength of vortex shedding, however, shedding frequency gradually decreases with CR. Hence, CV tube may be categorized by uni-agglomerating fluid structures. Although the vortex shedding frequency is high in all CVs, the amplitude of shedding is so small that the vortical structures seems non-fluctuating whose consequence can be observed in heat transfer with insignificant augmentation upto CV0.225. However, it is not mitigating due to the fact that the sideways shift of fluid structures fulfils the purpose of sweeping action of vortices. Nevertheless, a reasonably good augmenting heat transfer of CV0.3 occur that attributed to the huge shift and agglomeration of fluid structures towards the inner zone. When the curvature of the tube is made CX, the suction shifts outwardly with respect to central plane, so the agglomeration of fluid structures occurs near the ends of tube, hence, convex tube may be categorized by bi-agglomerating fluid structures. Consequently, a similar consequence as that of CV0.075 occurs on CX0.075 with distinct feature of shift of fluid structures away from the central plane. Hence, heat transfers of both cases are comparable with similar drag as well as frequency and strength of vortex shedding. The agglomeration becomes denser and denser with increase in CR exhibiting distinct vortex shedding frequencies of CX0.15, CX0.225 and CX0.3. Frequency as well as strength of vertex shedding was higher in CX0.15, low frequency and higher strength of vortex shedding holds by CX0.225, while high frequency and low strength of vortex shedding holds by CX0.3. As a result of the above phenomena a highly profound surface gliding occurs in CX0.15 and shows higher rates of heat transfer. A little bit lesser profound but reasonably good surface gliding action in CX0.225 shows somewhat lesser but reasonably good heat transfer rates, while least profound surface gliding mitigates the heat transfer in case of CX0.3.

3. Conclusions

A three-dimensional computational study of heat transfer capabilities of convex and concave type curved circular tubes based on direction of free stream of air have been compared with that of a straight tube. Four different curvature ratios have been taken i.e. 0.075, 0.15, 0.225, and 0.3. The tube surface was given constant heat flux condition and flow Reynolds number was maintained at 35000. The following conclusions have been summarized from the present investigation:

1. Three zones can be retained to conduct the comparative study viz. Zone of Augmented Influence (ZAI); Zone of Mitigated Influence (ZMI) and Zone of Insignificant Influence (ZII).
2. The flow structures can be categorized into two types based on the shift during its flow over the tube in the separated segmented surface as uni-agglomorating type or bi-agglomerating type.
3. Frequency and amplitude have great influence on heat transfer capabilities on the separated portion. Higher the amplitude higher will be the heat transfer rates.
4. Curvatures provided on the tubes augments the overall heat transfer, however, directional placement of curvature i.e. concave or convex manner with respect to free stream flow also influences the heat transfer capabilities from the tube surface. The present investigation showed that the highest thermal performance exhibited by CX0.15 followed by yet another good thermal performance by CX0.225 and CV0.3. The cases of CX0.075 and CV0.075 also show a better HTR compared to that of ST. The cases of CV0.15 and CV0.225 show insignificant thermal performance, while the case of CX0.3 does not show augmentation in thermal performance rather it shows mitigation having least profound surface gliding of flow structures.

DOI: 10.55214/25768484.v8i6.3757

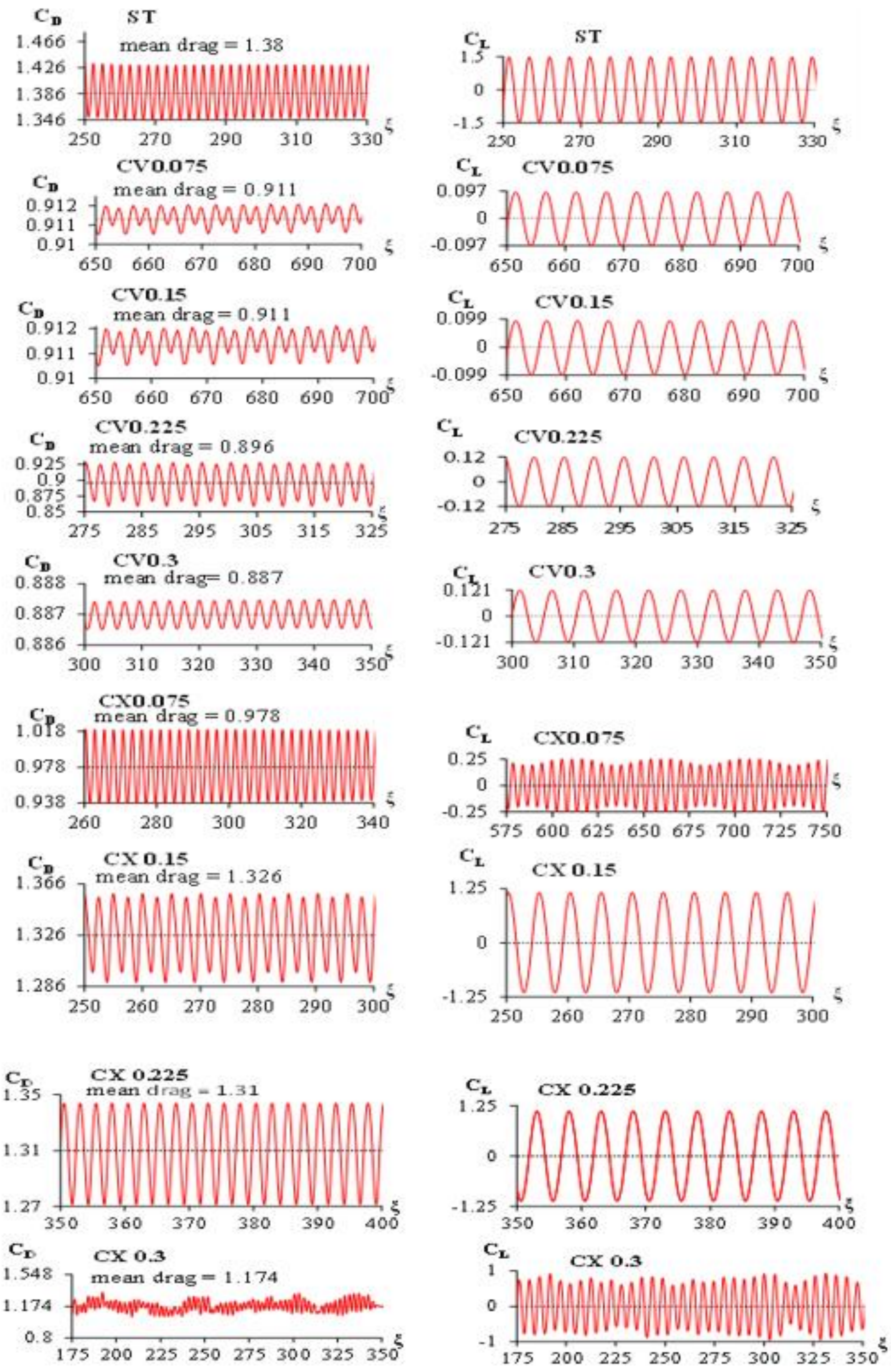

Figure 9.
Monitored data of drag and lift coefficients at different CR.

Edelweiss Applied Science and Technology
ISSN: 2576-8484
Vol. 8, No. 6: 8126-8149, 2024
DOI: 10.55214/25768484.v8i6.3757

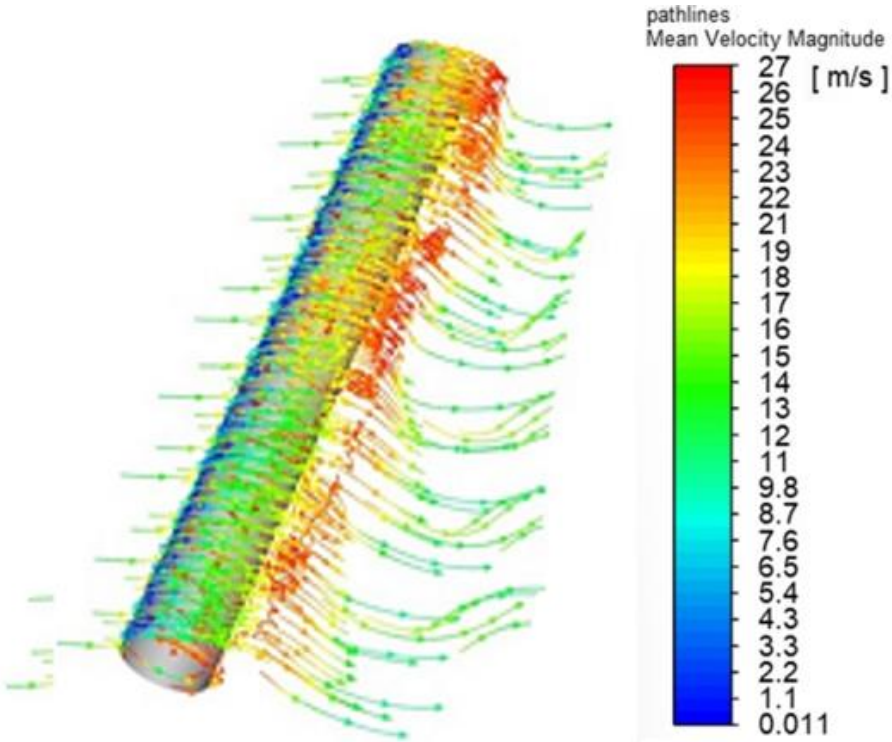

Figure 10(a).
Pathlines of velocity magnitude for straight tube.

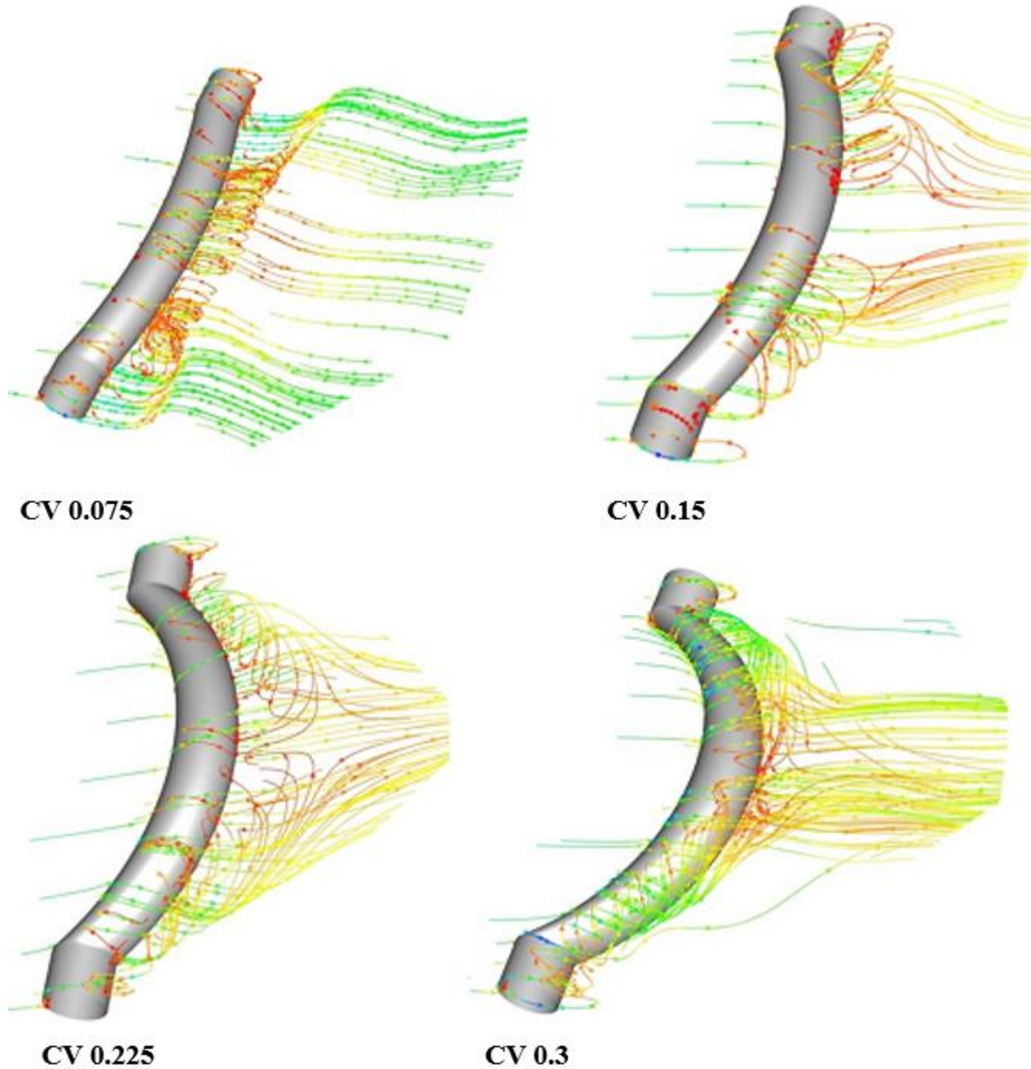

Figure 10(b).
Pathlines of velocity magnitude for curved tube with concave curvature.

ISSN: 2576-8484
Vol. 8, No. 6: 8126-8149, 2024
DOI: 10.55214/25768484.v8i6.3757

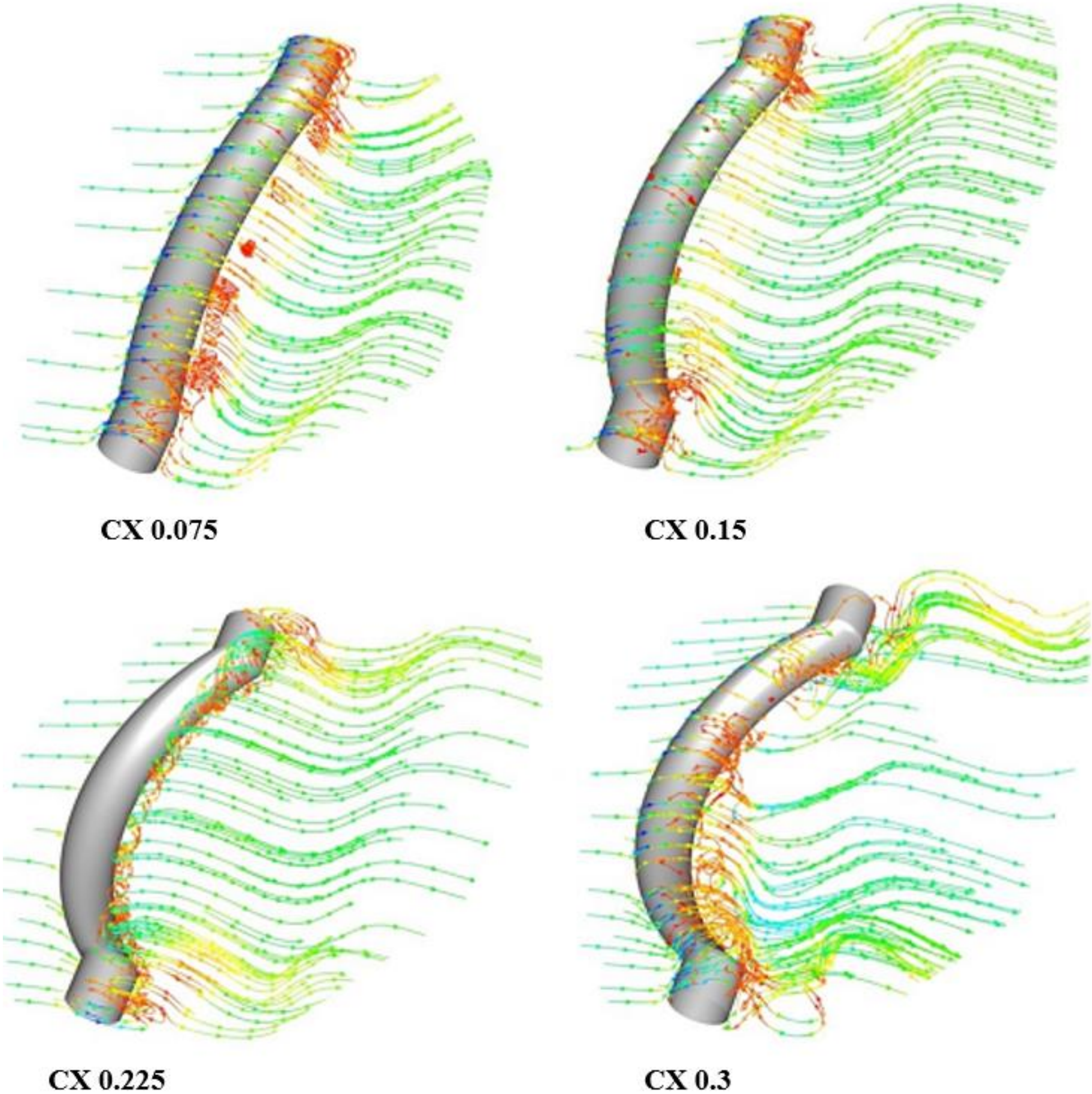

Figure 10(c).
Pathlines of velocity magnitude for curved tube with convex curvature.

Nomenclature:

Abbreviation

CR	Curvature Ratio
CV	Concave tube
CX	Convex tube
HTR	Heat Transfer Ratio
sf	Surface fraction
St	Strouhal number
ST	Straight tube
ZAI	Zone of Aggravating Influence
ZI	Zone of Influence

Symbols

c	Central deflection of the curved tube, m
C_D	Coefficient of drag
C_L	Coefficient of lift
C_P	Coefficient of pressure
D	Diameter of tube, m
F_x	Drag force, N
F_y	Lift force, N
h	Heat transfer coefficient, $Wm^{-2}k^{-1}$
H	End-to-end length of the tube, m

ZMI	Zone of Mitigating Influence	K	Thermal conductivity $Wm^{-1}k^{-1}$
		L	Chord length of curved segment of tube, m
		Nu	Nusselt number
Greek symbols		Nu_m	Time averaged mean Nusselt number
ν	Kinematic viscosity m^2s^{-1}	Nu_θ	Time averaged local Nusselt number
ρ	Density, kgm^{-3}	Re	Reynolds number based on tube diameter
ξ	Non-dimensional time	p_∞	Free stream pressure, Nm^{-2}
θ	Circumferential angle from geometric front stagnation point	u,v,w	Velocity components in x, y and z direction, respectively
		x	Streamwise coordinate
		z	Vertical coordinate

References

[1] P. Hishikar, V. K. Gaba, S. K. Dhiman and A. K. Tiwari, "Thermal performance of four cylinders in different layouts of spacing ratios under cross-flow at Reynolds number of 35000," Ocean Engineering, vol. 281, 2023. https://doi.org/10.1016/j.oceaneng.2023.114834

[2] A. Dhiman and R. Shyam, "Unsteady heat transfer from an equilateral triangular cylinder in the unconfined flow regime," International Scholarly Research Notices, 2011. https://doi.org/10.5402/2011/932738

[3] N. Mahir and Z. Altaç, "Numerical investigation of convective heat transfer in unsteady flow past two cylinders in tandem arrangements," International Journal of Heat and Fluid Flow, vol. 29(5), pp. 1309-1318, 2008. https://doi.org/10.1016/j.ijheatfluidflow.2008.05.001

[4] T. Abdelhamid, A. G. Rahma, M. M. Alam, R. Chen, M. Islam, Q. Zhou and H. Zhu, "Heat transfer and flow around curved corner cylinder: effect of attack angle," SN Applied Sciences, vol. 5(163), 2023. https://doi.org/10.1007/s42452-023-05377-w

[5] T. Ambreen and M. H. Kim, "Flow and heat transfer characteristics over a square cylinder with corner modifications," International Journal of Heat and Mass Transfer, vol. 117, pp.50-57, 2018. https://doi.org/10.1016/j.ijheatmasstransfer.2017.09.132

[6] S.A. Nada, H. El-Batsh and M. Moawed, "Heat transfer and fluid flow around semi-circular tube in cross flow at different orientations," Heat and Mass Transfer, vol. 43, pp.1157–1169, 2007. https://doi.org/10.1007/s00231-006-0202-y

[7] A. Mityakov, V. Mityakov, S. Sapozhnikov, A. Gusakov, A. Bashkatov, V. Seroshtanov, E. Zainullina and A. Babich, "Hydrodynamics and heat transfer of yawed circular cylinder," International Journal of Heat and Mass Transfer, vol. 115, pp. 333–339, 2017. http://dx.doi.org/10.1016/j.ijheatmasstransfer.2017.07.05

[8] A. Gau, J.M. Wu and C.Y. Liang, "Heat Transfer Enhancement and Vortex Flow Structure Over a Heated Cylinder Oscillating in the Crossflow Direction," ASME J. Heat Transfer, vol. 121, 789-795, 1999. https://doi.org/10.1115/1.2826067

[9] J. Ghazanfarian and M. R. H. Nobari, "A numerical study of convective heat transfer from a rotating cylinder with cross-flow oscillation," International journal of heat and mass transfer, vol. 52(23-24), pp.5402-5411, 2009. https://doi.org/10.1016/j.ijheatmasstransfer.2009.06.036

[10] S. Sanitjai,, and R. J. Goldstein, "Heat transfer from a circular cylinder to mixtures of water and ethylene glycol," International journal of heat and mass transfer, vol. 47(22),pp.4785-4794, 2004. https://doi.org/10.1016/j.ijheatmasstransfer.2004.05.013

[11] N. Srinil, "Analysis and prediction of vortex-induced vibrations of variable-tension vertical risers in linearly sheared currents," Applied Ocean Research, vol. 33(1), pp.41-53, 2011. https://doi.org/10.1016/j.apor.2010.11.004

[12] M. Chiatto, J. K. Shang, L. de Luca and F. Grasso, "Insights into low Reynolds flow past finite curved cylinders," Physics of Fluids, vol. 33(3), 2021. https://doi.org/10.1063/5.0043222

[13] F. Jiang, B. Pettersen, H. I. Andersson, "Influences of upstream extensions on flow around a curved cylinder," European Journal of Mechanics-B, Fluids, vol. 67, pp.79-86, 2018. https://doi.org/10.1016/j.euromechflu.2017.08.006

[14] J. P. Gallardo, B. Pettersen and H. I. Andersson, "Dynamics in the turbulent wake of a curved circular cylinder," In Journal of Physics: Conference Series, Vol. 318, No. 6, p. 062008, IOP Publishing, 2011. https://doi.org/10.1088/1742-6596/318/6/062008

[15] A. Miliou, J. S. Spencer and J. M. R. Graham, "Fluid dynamic loading on curved riser pipes," Journal of Offshore Mechancis and Arctic Engineering, vol. 125(3), pp.176-182, 2003. https://doi.org/10.1115/1.1576817

[16] Miliou, A. D. Vecchi, S. J. Sherwin and J. M. R. Graham, "Wake dynamics of external flow past a curved circular cylinder with the free stream aligned with the plane of curvature," Journal of Fluid Mechanics, vol. 592, pp. 89-115, 2007. https://doi.org/10.1017/S0022112007008245
[17] O. Yemenici and H. Umur, "Experimental aspects of heat transfer enhancement over various flow surfaces," Heat Transfer Engineering, vol. 37(5), pp. 435-442, 2016. https://doi.org/10.1080/01457632.2015.1057449
[18] O.F. Can, N. Celik and I. Dagtekin, "Numerical Analysis of External Flow Heat Transfer Around Slightly-Curved Surfaces," Arabian Journal for Science and Engineering, vol. 39, pp. 1219–1230, 2014. https://doi.org/10.1007/s13369-013-0675-1
[19] Y. Gao, J. He, M. C. Ong, M. Zhao and L. Wang, "Three-dimensional numerical investigation on flow past two side-by-side curved cylinders," Ocean Engineering, vol. vol. 234(15), 2021. https://doi.org/10.1016/j.oceaneng.2021.109167
[20] T. E. Aasland, B. Pettersen, H. I. Andersson and F. Jiang, "Flow Around Curved Tandem Cylinders," Journal of Fluids Engineering, vol. 144(12), p. 121301, 2022. https://doi.org/10.1115/1.4054890
[21] R. E. Mayle, M. F. Blair and F. C. Kopper, "Turbulent boundary layer heat transfer on curved surfaces," ASME Journal of Heat and Mass Transfer, vol. 101, 1979. https://doi.org/10.1115/1.3451021
[22] S. K. Dhiman, A. Kumar and J. K. Prasad, "Unsteady computation of flow field and convective heat transfer over tandem cylinders at subcritical Reynolds numbers," Journal of Mechanical Science and Technology, vol. 31, pp. 1241-1257, 2017. https://doi.org/10.1007/s12206-017-0223-0
[23] S. S. Paul, S. J. Ormiston and M. F. Tachie, "Experimental and numerical investigation of turbulent cross-flow in a staggered tube bundle," Journal of Mechanical Science and Technology, vol. 29(2), pp. 387-414, 2008. https://doi.org/10.1016/j.ijheatfluidflow.2007.10.001
[24] T. Tsutsui and T. Igarashi, "Heat transfer enhancement of a circular cylinder, ASME Journal of Heat and Mass Transfer," vol. 128(3), 2006. https://doi.org/10.1115/1.2150832
[25] H. Nakamura and T. Igarashi, "Variation of Nusselt number with flow regimes behind a circular cylinder for Reynolds numbers from 70 to 30 000," International journal of heat and mass transfer, vol. 47(23), pp. 5169-5173, 2004. https://doi.org/10.1016/j.ijheatmasstransfer.2004.05.034
[26] S. K. Dhiman, J. K. Prasad and A. Kumar, "Unsteady convective heat transfer in cross flow past two tandem cylinders: an inverse heat conduction approach," Heat and Mass Transfer, vol. 53(5), pp. 1761-1775, 2017. https://doi.org/10.1007/s00231-016-1927-x
[27] S. K. Dhiman, A. Kumar and J. K. Prasad, "Heat transfer by satellite cluster of cylinders at subcritical Reynolds number," Heat and Mass Transfer, vol. 55, pp. 595-612, 2019. https://doi.org/10.1007/s00231-018-2426-z
[28] T. Igarashi, "Characteristics of the flow around two circular cylinders arranged in tandem: 2nd report, unique phenomenon at small spacing," Bulletin of JSME, vol. 27(233), pp. 2380-2387, 1984. https://doi.org/10.1299/jsme1958.27.2380
[29] A. D. Roy and S. K. Dhiman, "Solutions of one-dimensional inverse heat conduction problems: a review," rans. Transactions of the Canadian Society for Mechanical Engineering, vol. 47(3), 2023. https://doi.org/10.1139/tcsme-2022-0157.
[30] S. K. Dhiman and J. K. Prasad, "Inverse estimation of heat flux from a hollow cylinder in cross-flow of air," Applied Thermal Engineering, vol. 113, pp. 952-961, 2017. https://doi.org/10.1016/j.applthermaleng.2016.11.088
[31] D. K. Walters and D. Cokljat, "A three-equation eddy-viscosity model for Reynolds-averaged Navier–Stokes simulations of transitional flow," vol. 130(12), p. 121401, Journal of Fluids Engineering, 2008. https://doi.org/10.1115/1.2979230
[32] Perkins, Jr, H. C., Leppert, G., "Local heat-transfer coefficients on a uniformly heated cylinder," International Journal of Heat and Mass Transfer, vol. 7(2), pp. 143-158, 1964. https://doi.org/10.1016/0017-9310(64)90079-1
[33] T. Igarashi, "Characteristics of the flow around two circular cylinders arranged in tandem," 1st report. Bulletin of JSME, vol. 24(188), pp. 323-331, 1981. https://doi.org/10.1299/jsme1958.24.323